Combustion and Flame 216 (2020) 271–279

Contents lists available at ScienceDirect

Combustion and Flame

journal homepage: www.elsevier.com/locate/combustflame

Role of dimethyl ether in incipient soot formation in premixed ethylene flames

Zepeng Li[a,b,c], Peng Liu[b,*], Peng Zhang[a,c], Yu Wang[d], Hong He[a,c,e], Suk Ho Chung[b], William L. Roberts[b]

[a] State Key Joint Laboratory of Environment Simulation and Pollution Control, Research Center for Eco-Environmental Sciences, Chinese Academy of Sciences, Beijing 100085, China
[b] King Abdullah University of Science and Technology (KAUST), Clean Combustion Research Center, Thuwal, Saudi Arabia
[c] University of Chinese Academy of Sciences, Beijing 100049, China
[d] School of Automotive Engineering, Wuhan University of Technology, Wuhan 430070, PR China
[e] Center for Excellence in Regional Atmospheric Environment, Institute of Urban Environment, Chinese Academy of Sciences, Xiamen 361021, China

ARTICLE INFO

Article history:
Received 8 January 2020
Revised 5 March 2020
Accepted 5 March 2020
Available online 3 April 2020

Keywords:
Premixed flame
Incipient soot
Particle size distribution
Dimethyl ether

ABSTRACT

Emissions of soot particles exert crucial impact on human health and the environment. Previous researches show that a partial replacement of fossil fuels with oxygenated fuels is supposed to reduce soot emission. However, the crucial information of soot size distributions is unclear, although small particles are more dangerous than large particles. In this paper, dimethyl ether (DME) is selected among the oxygenated fuels for the investigation of the doping effect on nascent soot formation. DME was doped in the burner-stabilized rich premixed ethylene/oxygen/argon flames at various mixing ratios. Flame temperature profiles were measured using R-type thermocouples with radiation correction. A scanning mobility particle sizer (SMPS) with a sampling system was used to determine particle size distributions (PSDs) of soot-containing combustion products with immediate dilution. Thermo-gravimetric analysis (TGA) complemented with elemental analysis (EA) was conducted to detect the chemical properties of formed soot particles. Additionally, species profiles of the experimental flame conditions were provided from simulations. The experimental PSDs showed that DME addition could slow down soot evolution process, while lead to a slight increase in incipient soot with size below 4 nm. When DME added, the production of benzene was suppressed due to the reduced concentrations of acetylene and propargyl, and thus soot nucleation. Meanwhile, soot oxidiation was enhanced because the OH radical and the oxidizability of soot particles are both increased. Considering the slight increase of sub-4 nm soot, the effect of oxygenated-PAHs (OPAH) was emphasized. The production of OPAH suppressed soot surface growth, which leading to the relatively lower consumption of sub-4 nm soot in DME added flames.

As a result, DME cannot be simply regarded as a clean fuel due to the enhanced formation of sub-4 nm soot particles. When applying oxygenated fuels into practice, it is necessary to pay more attention to the size distributions of the emitted particles, and conduct appropriate post-processing techniques to reduce the emissions of small particles.

1. Introduction

Oxygenated fuels including several biofuels in practical combustion systems have attracted significant research interests in recent years, as a result of the consensus to mitigate emission and reduce the energy dependence on conventional fossil fuels. A partial replacement of fossil fuels with oxygenated fuels contributes positively to address present concerns of energy security and environmental pollution [1–4]. In particular, the emission of combustion-generated soot particles, which not only poses great hazards to human health but plays a vital role in climate change [5,6], could be mitigated by using oxygenated fuels.

Quantitative estimations of sooting tendencies of oxygenated and regular hydrocarbon fuels have been extensively investigated with the yield sooting index (YSI), and the sooting tendencies are

* Corresponding author.
E-mail address: peng.liu.1@kaust.edu.sa (P. Liu).

https://doi.org/10.1016/j.combustflame.2020.03.004
0010-2180/

significantly inhibited in oxygenated fuels added to methane/air non-premixed flames compared to those of other additives [7]. However, numerous studies show that some of the oxygenated "clean" fuels may not be clean in some cases [8–10]. Manufactured from methane or coal gasification, dimethyl ether (DME) is considered as a promising alternative fuel or fuel additive for clean combustion [11–15]. Interestingly, different effects of DME addition on soot formation were observed in premixed and non-premixed flames. Wu et al. investigated the addition of DME on polycyclic aromatic hydrocarbon (PAH) and soot formation in a fuel-rich ethylene flame using laser-induced incandescence (LII) and laser-induced fluorescence (LIF) techniques [16]. Their results revealed that the both PAH and soot signals decreased with DME addition. This conclusion was further comfirmed by Mariano et al. via monitoring the PAH and soot concentrations using LII and LIF methods [17] and Kang et al. by simulating an ethylene premixed burner-stabilized stagnation flame with DME addition [18]. In non-premixed counterflow ethylene flames, a non-monotonic variation of soot volume fraction (i.e., synergistic effect) was experimentally observed with the increase of the DME doping ratio [8,9]. In particular, both benzene and soot formation were enhanced with up to 10% with DME addition in non-premixed coflow ethylene flames [10]. Similar phenomenon was observed in larminar coflow ethylene diffusion flames by Liu et al. [19–20] and Beth et al. [21]. However, the papers cited above mainly focus on soot volume fraction measurement using laser-based diagnosis methods. To our best knowledge, the size distribution information of soot in DME doping flames is unclear.

Many parameters or variables should be used together to determine if a fuel or fuel additive is clean or not. Besides total emission, the size distributions, chemical compositions, and nanostructures of soot particles contribute more to their toxicity [22,23]. Regarded as low sooting tendency fuels, some oxygenated fuels were evidenced to enhance the formation of small nascent soot. In lab-scale flames, there was a slight increase of soot with sizes less than 3 nm in ethylene premixed flames doped with 10% of ethanol [24,25]. And in an engine test bench, it was observed that the emission of particles with sizes less than 25 nm was increased, as the proportion of oxygenated additives such as ethyl tert-butyl ether (ETBE, $C_6H_{14}O$) and diglyme ($C_6H_{14}O_3$) increased [26]. Conversely, doping the high sooting tendency fuel benzene into premixed ethylene flame led to the decrease of particles with sizes less than 10 nm, while the production of large aggregates larger than 100 nm increased [27]. Therefore, considering the real toxicity of particle emissions, it is vital to investigate the effect of DME addition on the emissions of small soot particles (<4 nm), which is beyond the detection limit of LII method.

In this study, the soot evolution process with DME addition is systematically investigated. Consider that the information of the flame thermal field and soot size distributions as functions of residence time is vital in the analysis of soot evolution process, and premixed laminar flames are frequently used to provide the aforementioned information. In this regard, a burner-stabilized premixed flame with well-defined boundary conditions was carried out in this work. Temperature profiles were measured using thermocouples to provide the thermal variations in DME added premixed ethylene flames. Particle size distributions (PSDs) were measured to show the impact of DME in emitted soot size as well as the soot evolution process, especially the "smallest" soot at soot nucleation stage. Thermo-gravimetric analysis (TGA) complemented with elemental analysis (EA) were conducted to detect the chemical property of formed soot particles, thus deduce the DME effect on soot elemental composition and oxidation process. Kinetic simulations were also conducted to discuss the concentration profiles of some important intermediates to support the experimental information.

Table 1
Experimental conditions for ethylene/DME flames at $\phi = 2.0$.

Flame	Cold gas velocity, V_0 (cm/s)	Fuel composition (%)		Peak temperature (K) at $H_p = 1.2$ cm
		DME	C_2H_4	
A1	6	0	100	1787.65
A2		10	90	1800.48
A3		20	80	1808.71
A4		30	70	1814.56
B1	8	0	100	1857.82
B2		2	98	–
B3		5	95	–
B4		10	90	1864.81
B5		20	80	1872.81
B6		30	70	1877.48

2. Methodology

2.1. Experimental methods

2.1.1. Flame configuration

The laminar premixed flames investigated in this study were established on a commercially-available Mckenna burner, which consisted of a central cylindrical porous sintered matrix (diameter of 6 cm) for uniform outflow of fuel/oxidizer premixture and a surrounding annular passage for N_2 shield. The sooting post-flame zone of the premixed flame was made stable by using a stagnation plate placed above the burner, which also served to provide a well-defined boundary condition amenable to numerical simulation. Both the burner and the stagnation plate were cooled by recirculating water. An unburned reactant composition of fuel: oxygen: argon was 16: 24: 60% mol (equivalence ratio of $\phi = 2.0$). The fuel composed of ethylene (C_2H_4) and DME(C_2H_6O) with the DME mixing ratio ranging from 0 to 30% with pure ethylene being the baseline case, thus all the test were at the same total carbon feed. Atmospheric pressure flames were tested for two cold gas velocities V_0. The flowrates of the gases were controlled by thermal-based mass flow controllers (MFC, MKS Instruments), which were calibrated by a piston-driven dry gas flow calibrator (Definer, 220). Detailed experimental conditions are summarized in Table 1.

2.1.2. Temperature measurement

Temperature profiles were measured using thermocouples with a rapid insertion technique coupled with a radiation correction, as detailed in [28–31]. A R-type thermocouples (wire diameter of 0.25 mm) was coated with silica to prevent surface catalysis effect having the bead diameter of 0.3 mm. The emissivity of R-type thermocouples was 0.22 ± 0.02 (≈1400 K) [32]. Since the residence time of the thermocouples was rather short and the flames were only moderately sooting, the soot emissivity was not considered in the overall emissivity. Then, the energy balance equation becomes:

$$\varepsilon\sigma T_j^4 = \frac{k_{g,0}Nu_j}{2d_j}\left(T_g^2 - T_j^2\right)$$

where T_g is the true gas temperature, and T_j is the junction temperature, ε is the overall emissivity of the thermocouples, σ is the Stefan-Boltzmann constant, $k_{g,0} = \frac{k_g}{T_g}$ and k_g is the thermal conductivity of local gas, d_j is the diameter of the thermocouple junction. Nu_j is the Nusselt number with $Nu = 0.34 + 0.65 \times Re^{0.45}$ [33], where Re is the Reynolds number. Local gas properties such as viscosity and thermal conductivity were calculated using TRANSPORT package [34].

2.1.3. Particle size distribution measurement

The experimental procedure for the measurement of soot size distributions followed the previous works of Abid et al. [35] and Camacho et al. [36]. The scanning mobility particle sizer (SMPS) system consisted of an electrostatic classifier (TSI, Model 3087) and an ultrafine condensation particle counter (TSI, Model 3776). The soot-containing combustion products were sampled through a 150 μm orifice drilled through the surface of stainless-steel tube, which was in turn horizontally embedded into the stagnation plate and served as a sample transfer line from the flame to the analyzing instrument. A controllable (through the needle valve) vacuum was generated in the sampling tube by a vacuum pump to induce the reaction products in. To avoid soot aggregation and minimize particle loss (due to diffusive wall deposition) in the transfer line, immediate dilution by filtered N_2 was applied. The flow rates of dilution N_2 gas were controlled by an MFC at 28 L/min (STP). The sample and sheath flow rates through the DMA were set at 1.5 and 15 L/min, respectively. The scan time of the SMPS was 50 s up and 10 s down and after each scan, the orifice in the sampling tube was cleaned using a fine wire to minimize the impact of the accumulation of soot particles around the rim of the orifice.

As the flow rate of the dilution N_2 was fixed, the sample dilution ratio was determined as a function of the amount of product gas that was withdrawn, which was dependent on the pressure drop (Δp). Δp could in turn be controlled by the level of vacuum in the sampling tube. The technique described in [37] was utilized to optimize the dilution ratio, and all experiments were conducted using the same dilution ratio. In this condition, a normalized number density (NND) was presented to compare the impact of various DME addition on soot size distribution, defined as: $\mathrm{NND} = (\frac{dn}{d\log D_p})\frac{1}{N}$, where D_p is the particle diameter and N is the total number density. Besides, due to the limitation of the Cunningham slip correction [38], a parameterized correlation was applied for the mobility diameter as described in [39]. To validate the present experimental setup and data processing procedures, the particle size distribution functions of a benchmark flame (Flame B1) was compared between this work and the work of Camacho et al. [36].

2.1.4. Characteristics of sampled soot

To study the effect of DME addition on the oxidation characteristics of soot particles, soot samples physically scraped from the stagnation plate were collected and analyzed for Flame series A. A thermo-gravimetric analyzer (TGA; TA Instruments, Q5000) was used to heat the soot samples in the N_2 atmosphere from room temperature to 300 °C at a rate of 2 °C/min, and isothermally at 300 °C for 10 minutes to desorb volatile compounds such as water vapor. Afterward, the N_2 atmosphere was changed to air for the oxidation of the soot samples at the heating rate of 1 °C/min from 300 to 700 °C. For further interpretation of the oxidation properties, the elemental composition of soot samples was acquired using the CHNS/O Analyzer (Thermo Scientific, Flash 2000). The calibration curves of different elements were tested by standard chemicals (sulfanilamide, BBOT, and acetanilide). Since the samples were free from ash, the content of oxygen (O) was calculated by subtracting the contents of C and H from 100%.

2.2. Simulations

Simulations were conducted for the investigated flames to provide insights to the experimental observations. The flame temperature profiles and species concentrations were computed with the burner-stabilized stagnation flame module in the CHEMKIN PRO package [40]. Transport properties such as gas-phase viscosities, conductivities, and diffusion coefficients were calculated using TRANSPORT package [34]. The chemical kinetics model employed here was KAUST-Aramco PAH Mech [41], where the KAUST PAH sub-mechanism was merged with NUIG's C0-C3 hydrocarbon sub-mechanism (i.e., AramcoMech 1.3 [42]) and the KAUST C1-C3 alcohol sub-mechanism. The base mechanisms including DME oxidation were validated against the DME/O_2/N_2 flames. The inlet boundary temperature was set as room temperature, and the downstream boundary temperature at the stagnation plate was set as 445 K as measured.

3. Results and discussions

3.1. Temperature profiles with DME addition

We first present the results on the measured temperature profiles considering that temperature is one of the most important parameters affecting the rate of soot formation/oxidation. It is therefore important to check the effect of DME addition on flame temperature before its influence on soot size distribution is discussed. Collecting samples at different heights above the burner surface require varying the location of the stagnation plate, which in turn change the downstream boundary conditions and temperature profiles. As such, the effect of stagnation plate position on flame temperature needs also to be determined to facilitate the analysis of the evolution of soot PSDs in flames.

Figure 1 shows the measured and computed temperature profiles in terms of the height above burner (HAB) at various burner-stagnation plate separation distances (H_p) of flames B1 (pure ethylene flame) and B6 (70% ethylene and 30% DME), respectively. Note that due to the finite size of the thermocouple junction, it is not possible to measure the temperature at positions very close to the burner surface. The spatial uncertainty for the temperature measurement is ±100 μm (estimated from the finite thermocouple diameter), and the temperature uncertainty is considered to be due primarily to the emissivity of the thermocouples. The measured temperature profiles agree well with the model prediction when the height above burner is less than 2 mm, but have obvious discrepancy for large distances, especially when H_p increases. This could be partially attributed to the insufficient consideration of the soot radiative heat loss to the surrounding in the simulations, which is increasingly severe at higher H_p due to the amount of soot produced. And the uncertainties in specifying the downstream temperature boundary condition may also play a role. Nevertheless, the essential features of the DME addition / stagnation plate position effects were well captured by the numerical simulations.

For a better comparison of the influence of DME addition on the flame temperatures, the experimental and computational peak flame temperatures as a function of DME mixing ratio for $H_p = 1.2$ cm are illustrated in Fig. 2 (see also Table 1). The maximum discrepancy between the numerical and experimental temperatures is around 16 K, which are within the uncertainty of the experiment. With the increase of the DME mixing ratio, the peak flame temperatures are increased monotonically. This may seem inconsistent at first glance, as the adiabatic flame temperature (AFT) calculation shows that AFT of ethylene (2521.7 K) is higher than that of DME (2264.3 K). The peak temperature is mainly determined by the heat release from combustion. Note that the equivalence ratio of the experimental flames is 2, thus the combustion is not complete for all flame cases. As DME added to the ethylene flames, more ethylene and DME were burnt so more heat is released. It is supposed to be the main contributor to the increase in T with DME addition. Note that the variation of the measured peak flame temperature with respect to DME addition in each series is less than 40 K, which is around 2% of the peak temperature. The small variation of peak flame temperatures suggests that the thermal effect by DME addition may not play an important role.

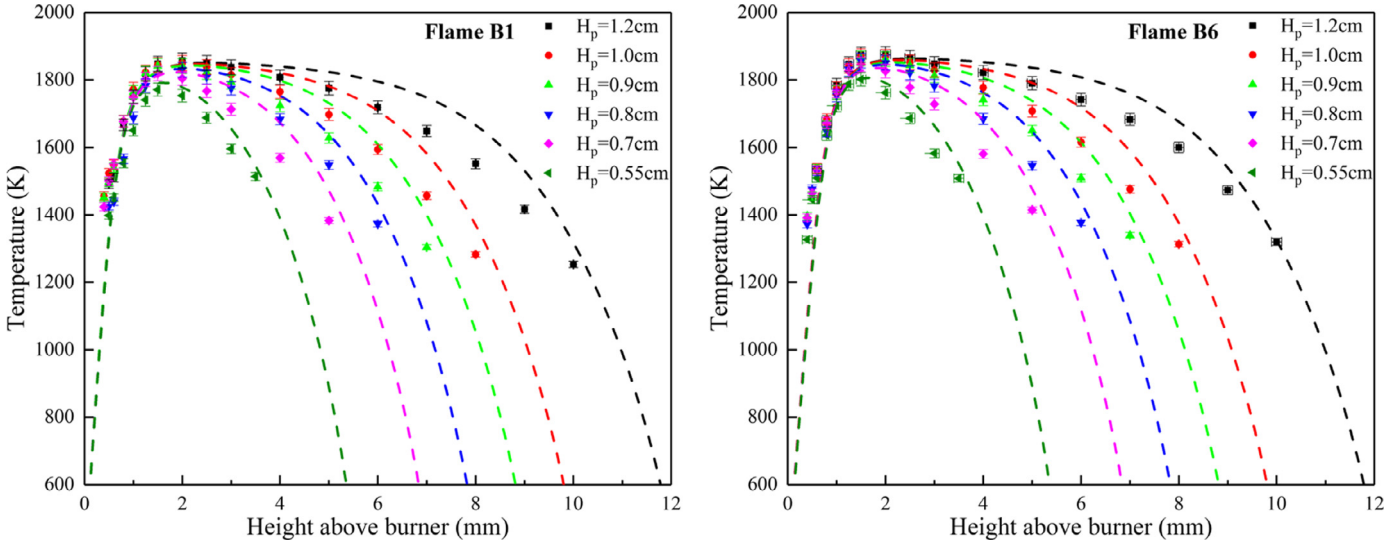

Fig. 1. Temperature profiles in terms of the height above burner surface at various separation distances in Flame B1 and B6. The points refer to the experimental data and the dashed lines refer to the simulation results.

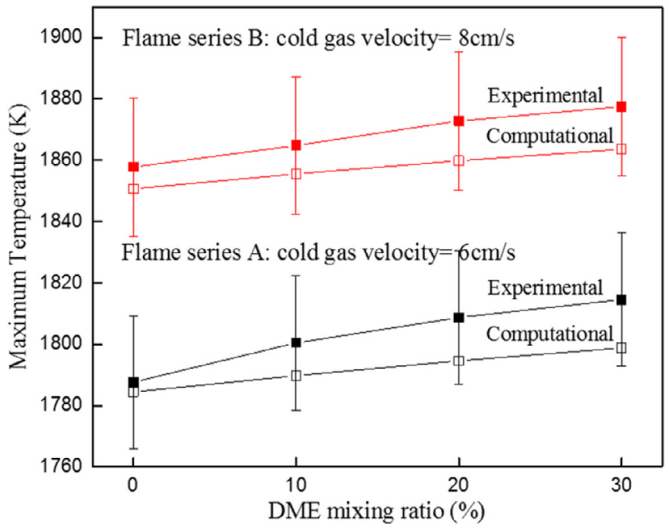

Fig. 2. Comparison of maximum experimental (solid symbols) and computational (hollow symbols) temperatures for H_p = 1.2 cm in terms of DME mixing ratio in Flame series A and B.

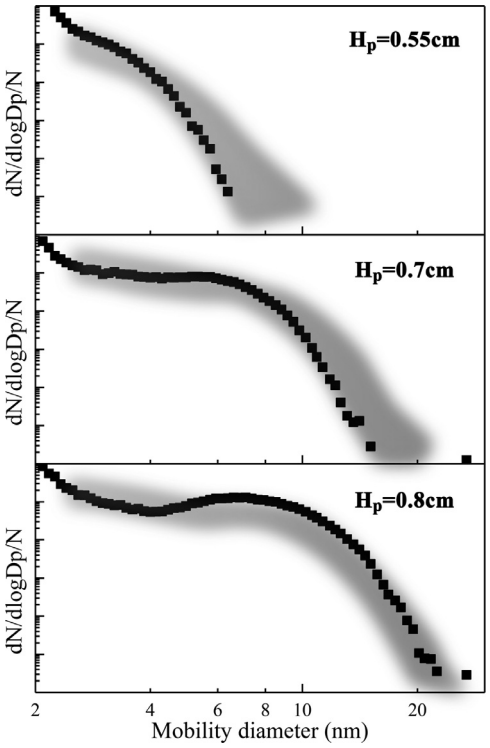

Fig. 3. Comparison of normalized PSDs of the benchmark flame B1 between this work (points) and [36] (shaded region).

3.2. Soot size distribution by DME addition

Before delving into the detailed results on soot PSDs of premixed flames of ethylene/DME mixtures, it is critical to confirm the reliability of our experimental data. This is especially important considering that there are many subtleties involved in the experimental procedures of PSD measurements using SMPS systems, including sampling orifice blockage and dilution ratio control. Figure 3 shows the comparison of the normalized PSDs of the benchmark flame (Flame B1) between this work and the multi-university collaborative SMPS work using similar apparatus by Camacho et al. [36]. The points are the experimental results at H_p = 0.55, 0.7, and 0.8 cm in this work. The shaded region covers the region of the mobility PSDs measured at 4 facilities in Camacho's paper, and the corresponding H_p = 0.45, 0.55, and 0.6 cm. Note that there are the distance offsets of 0.1–0.2 cm. These offsets may come from the different thicknesses of the sampling tube, or the different flow fields due to the apparatus hardware (MFCs, burner material, and pore distribution, etc.). Overall, it shows that the setup involved in this study can reproduce the evolution (monotonic to bimodal distribution) of the shape of the PSDs well except spatial offsets of separation distances.

The comparison of the normalized PSDs among flames with various DME mixing ratios, taken at several specific heights above the burner, is presented in Fig. 4. The black symbols represent the baseline case without DME mixing (Flame A1). As can be seen, soot starts to be detected at H_p = 0.55 cm. Subsequently, the shoulder or a distinct bimodal distribution appears at H_p = 0.8 cm, which result from the competition between the generation of small particles and consumption by surface reaction and coagulation among particles. If the height continues to increase to H_p = 0.9 cm, the

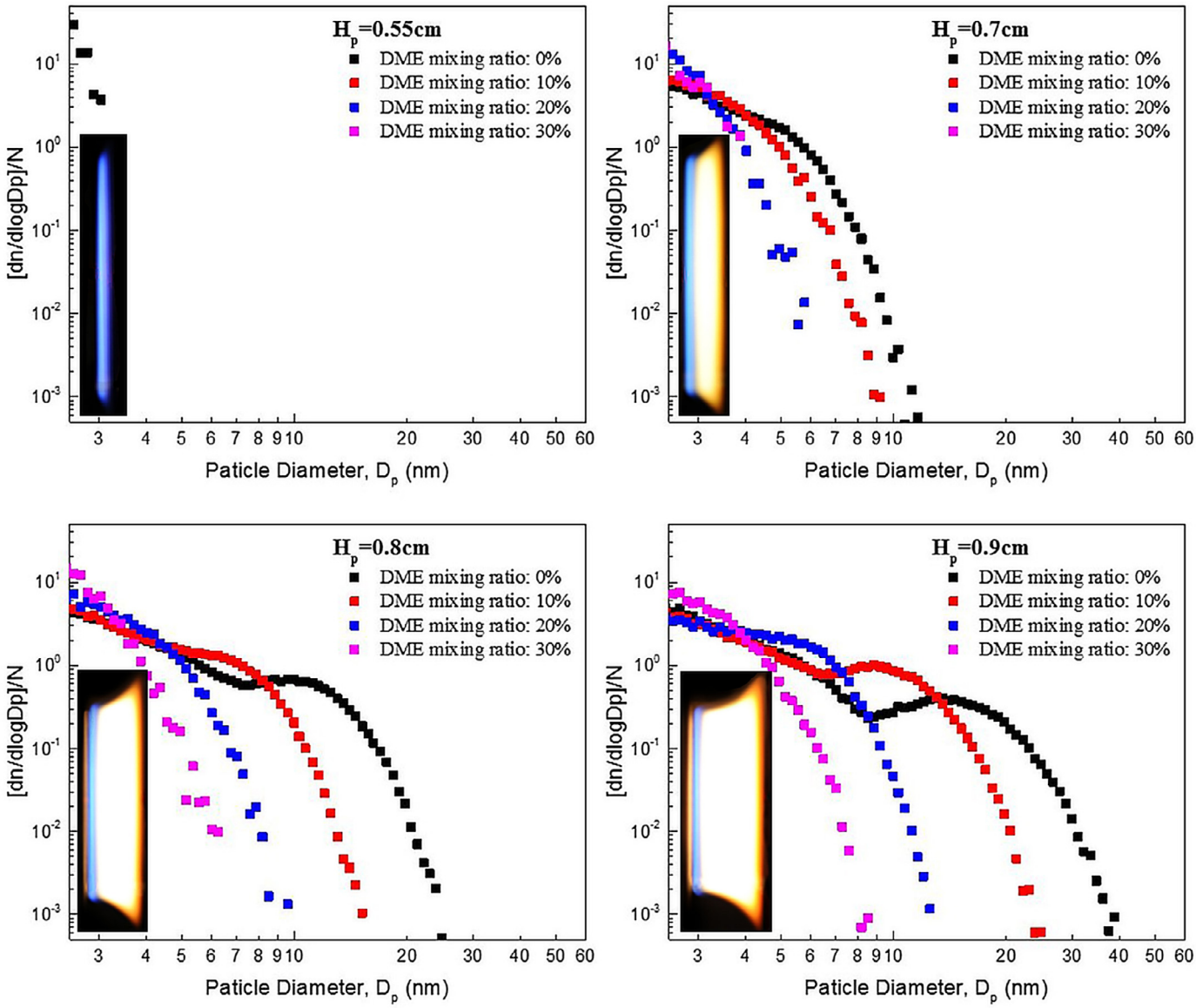

Fig. 4. Normalized PSDs at several separation distances in Flame series A.

domination status of soot nucleation decays and as H_p further increases, the PSD would transform into a unimodal distribution, however which can be outside the range of this observation. The effect of DME addition can be inferred from the specific height (H_p) for a certain proportion of soot sizes. For instance, producing certain proportion of soot with size around 9 nm, the required heights (H_p) are < 0.7, 0.7, 0.8, and 0.9 cm for the flames mixing with 0, 10, 20, and 30% DME, respectively. Considering the separation distance represents the residence time of soot, it implies an extended time is needed for soot production ascribed to DME addition. That is, doping DME slows down the evolution process of soot particles.

Nevertheless, a slight increase of small soot with sizes less than 4 nm is noted in DME added flames, as compared to that of the pure ethylene flame. Similar phenomenon was found in the studies of ethanol added ethylene flames by D'Anna and coworkers [24–25], where it was attributed to the lower progression of size and aromaticity of soot particles. In their studies, there is no information of size distributions of flame with ethanol addition less than 10%, while Yan et al. [43] found the synergistic effect (small amounts of doping of lower sooting-tendency fuel may increase soot or PAH formation of higher sooting-tendency fuel) of ethanol adding into counterflow diffusion flame of ethylene when addition <10% of ethanol. Since there is also a study of the synergistic effect when <10% of DME mixing in counterflow diffusion flames [9], more details of the variation of the PSDs with respect to the amount of DME addition are obtained in lower soot loading flames (Flame series B). Figure 5 presents the normalized PSDs with different DME mixing ratios in Flame series B. It is notable that 2% of DME addition has minimal impact on soot, and as DME mixing ratio increases, soot evolution slows down monotonically and continuously with an enhanced formation of soot smaller than 4 nm up to 20% DME. It is also noted that the relative soot volume fraction and number density decrease as functions of DME mixing ratios at various separation distance in Flame series B, as shown in Fig. 6.

3.3. Effect of DME addition on soot evolution

3.3.1. Slow-down effect of DME addition on soot process

Benzene (C_6H_6) can be considered as an important step for soot particle formation, and thus regarded as one of the important indicators of soot formation. Numerical simulations are performed

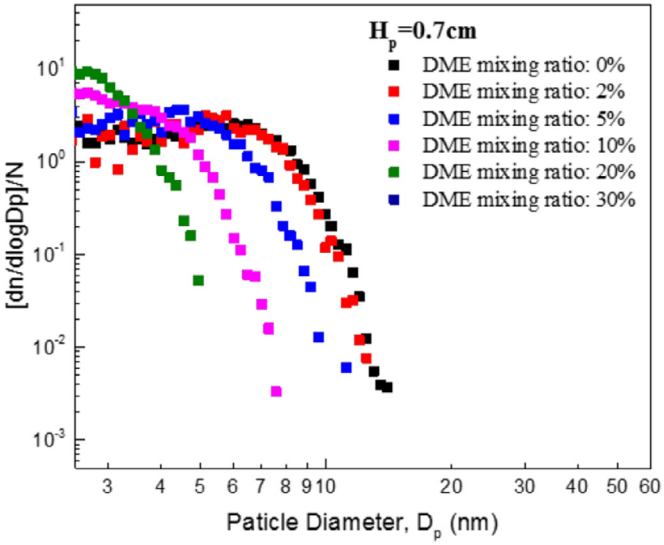

Fig. 5. Normalized PSDs with different DME mixing ratios in Flame series B.

to clarify the chemical effect of DME addition on soot formation. The prediction of the mole fractions of benzene is investigated as a function of height above burner surface for $H_p = 1.2$ cm in Fig. 7a. And the overall trend of naphthalene, phenanthrene, and pyrene is the same with benzene, which is shown in Fig. 7c. Note that the qualitative trends of concentrations of the investigated species are similar for Flame series A and B. The mole fractions of propargyl (C_3H_3), acetylene (C_2H_2), methyl (CH_3), and hydroxyl (OH) radicals are shown for Flame series B in Fig. 7b. It is obvious that as DME mixing ratio increases, mole fractions of benzene and investigated PAHs decreases. It is reasonable as the mole fractions of propargyl, and acetylene decrease with DME addition, since $C_4 + C_2$ and $C_3 + C_3$ reactions are expected to be the dominant pathways leading to benzene formation in ethylene flames. The mole fraction of methyl radical increases as DME addition, however it cannot compensate the benzene loss although methyl radical may promote the benzene formation via prompting the C_3H_3 formation [9]. Additionally, an enhanced oxidation behavior may also contributes to the benzene loss, as the OH radical is increased in DME added flames. Combined with above experiment results, where the concentration of small soot particle (<4 nm) increases with DME addition, it can be concluded that the benzene, or the small PAHs, are not suitable to be the sole indicator of soot particle due to their opposite trend in this study, at least for small soot particles.

In this regard, the oxidation characteristics of soot particles is studied with the TGA. The conversion (α) and the conversion rate ($d\alpha/dt$) are the typical parameters used to quantitatively describe the oxidation behaviors of the samples. The conversion is defined as $\alpha = \frac{M_0 - M_T}{M_0 - M_L}$, where M_0 is the dried sample weight after a 10-minute isothermal process at 300 °C, also regarded as the initial weight of soot samples; M_L is the weight of the leftover after complete oxidation and in the present study $M_L = 0$, since there was no leftover after TGA oxidation process; M_T is the weight of partially oxidized samples at temperature T. For better illustration of the influence of DME on the oxidation behaviors of soot particles, the critical temperatures at which 5, 50 and 95% soot particles are oxidized are compared in Fig. 8a. Obviously, as DME mixing ratio increases, the corresponding temperature indices decrease. That is, the addition of DME results in the soot particles being oxidized at lower temperature and thus the oxidation process being faster. It indicates the enhanced oxidation reactivity of soot samples derived from the DME mixing flames, or the decrease of soot resistance to be oxidized during soot formation or maturation processes. Therefore, more soot particles are consumed during oxidation process, which could contribute to the decrease of the total amount of emitted soot.

Figure 8b shows the mass ratios between oxygen (O) and hydrogen (H) to carbon (C). It is apparent that the increasing DME mixing ratio gives rise to the augment of O/C and H/C mass ratios for both Flame series A and B. The O/C ratios suggest that soot with more DME added should be easier to be oxidized as it has a higher amount of oxygenates per C atom [44]. Song et al. [45] mentioned that the incorporation of greater surface oxygen led to faster oxidation and more drastic structural transformation during soot oxidation process, and the role of surface oxygen groups was more important than their structure and pore size distributions. Meanwhile, the higher H/C ratio may associate with a higher concentration of active C–H sites, available for soot surface reactions [46]. Therefore, it will facilitate the production

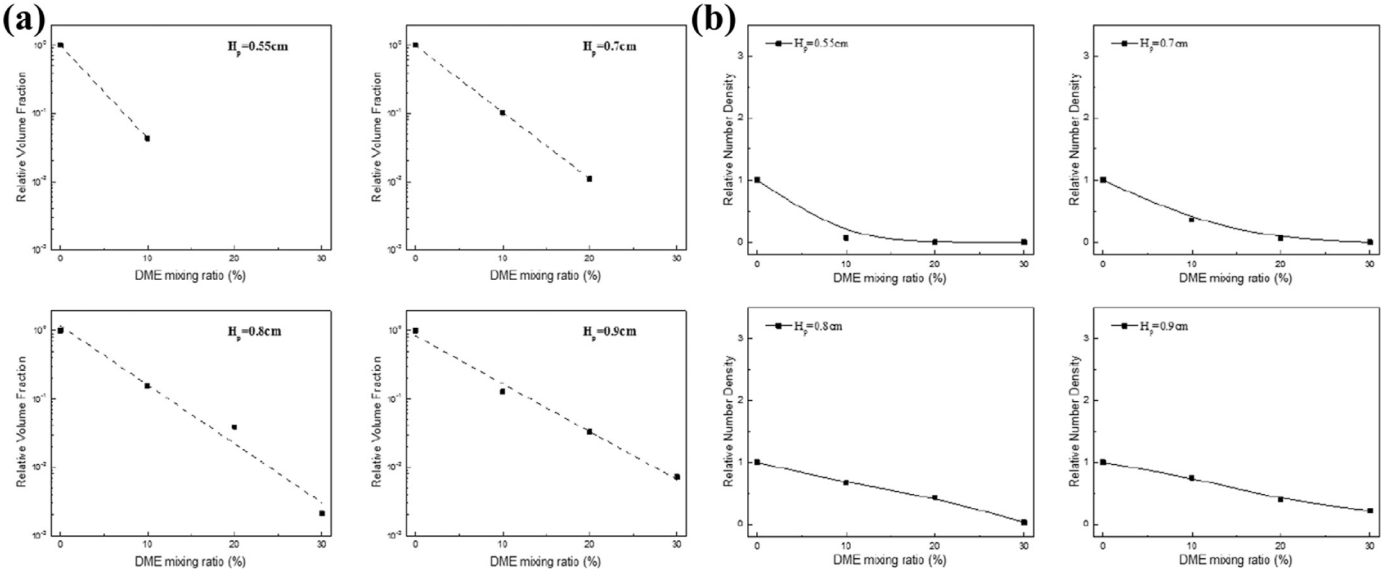

Fig. 6. Relative soot volume fraction (a) and number density (b) as a function of DME mixing ratios at various separation distance in Flame series B. Lines are fitted to the data.

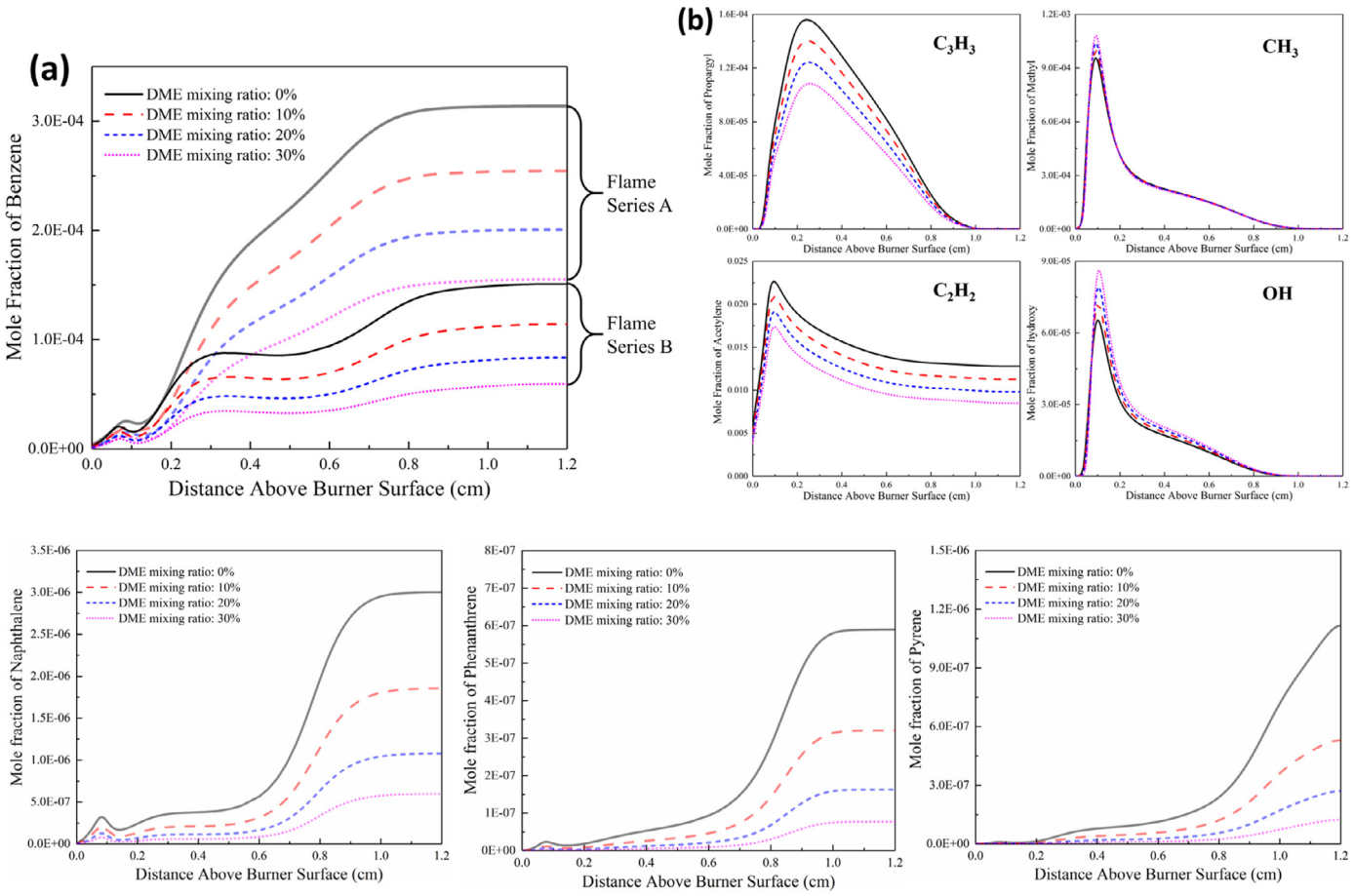

Fig. 7. Calculated axial profiles of the mole fractions profiles at H_p = 1.2 cm: (a) benzene (C_6H_6) of Flame series A and B; (b) propargyl (C_3H_3), acetylene (C_2H_2), methyl (CH_3), and hydroxyl (OH) radicals of Flame series B; (c) naphthalene, phenanthrene, and pyrene of Flame series B.

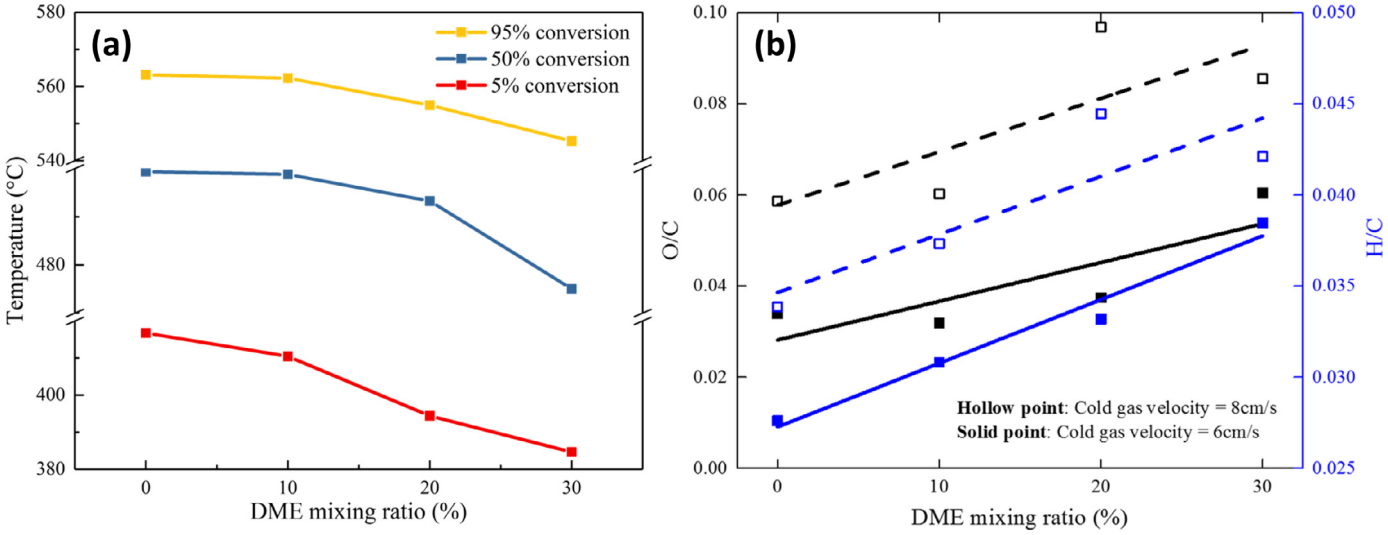

Fig. 8. Conversion temperatures (a) and O/C (black) and H/C (blue) mass ratios (b) of soot samples with increasing DME mixing ratios. (For interpretation of the references to color in this figure legend, the reader is referred to the web version of this article.)

of radical sites attacked by oxygen, which leads to the increase in soot oxidation rate. Overall, the stronger oxidation behavior of soot samples of DME added flames was experimentally supported by O/C and H/C mass ratio data. Additionally, the surface/volume ratio of soot particles increases with DME addition due to the decreased mean particle diameter, which also contributes to the increase of the oxidation rate.

3.3.2. *Increase of sub-4 nm soot of DME added flames*

Based on the above analyses, the soot formation becomes weak with DME addition due to the lower benzene concentration, and the soot oxidation is enhanced with more hydroxyl radicals (refer to Fig. 7) and higher oxidizability. It reasonably explains the slow-down effect on soot evolution with DME addition. While the increased nascent soot with size of sub-4 nm seems to be

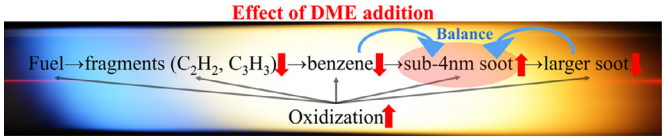

Fig. 9. Schematic of the effect of DME addition on the early stage of soot evolution. Red arrows indicate increasing and decreasing trends with DME addition. (For interpretation of the references to color in this figure legend, the reader is referred to the web version of this article.)

contradictory to this explanation. Figure 9 shows a proposed schematic of the effect of DME addition on the early stage of soot evolution. In the early stage of soot evolution process, fuel and oxidizer pyrolyzed into small fragments such as CH_2, CH_3, C_2H_2, C_3H_3, H, O, OH, etc. Among these fragments, C_2H_2, C_3H_3 are important in the formation pathways of benzene, and their concentrations decrease with DME doping. Then the formation of benzene is suppressed due to the lower production of its precursors. Subsequently, the formation of soot nuclear with size < 4 nm should be reduced due to the reduction of its precursor, but actually it was increased.

To elucidate the underlying mechanism of this phenomenon, the molecular structure of soot nucleus with size less than 4 nm should be figured out. Commodo et al. [47] reported an insight into the onset of the soot nucleation process using high-resolution atomic force microscopy (HR-AFM). Soot samples were collected in a premixed ethylene/air flame and at the height that the PSD presenting a mono-model distribution, where particle size was mostly between 2–4 nm. Their results indicated that the hydrocarbon species with 24–30 C-atoms were the main molecular constituents of the sampled soot with sizes of 2–4 nm. Thus, it is understandable that soot nucleation is suppressed by DME addition due to the reduced PAH concentration as shown in Fig. 7. However, during the growth process from soot nuclear (sub-4 nm soot) to larger soot particles, the role of oxygenated-PAH (OPAH) should be emphasized. The existence of OPAH in the formed soot from our experiments can be supported by two evidences: first, the increased oxygen content in soot samples from flames with higher DME mixing ratios, as shown in Fig. 8b; second, the detected C-O-C and C=O bonds from soot particles in a comparable premixed ethanol/ethylene flame using Fourier Transform Infrared Spectra (FTIR) [25]. OPAH is inclined to be formed on incipient soot surface, thus it mainly affects the surface reactions of soot particles [48]. The existence of OPAH inhibits soot surface growth process because of the relatively high energy barrier for the addition reactions: for instance, the energy barrier for the addition reaction of PAH radical with C_2H_2 is 2–3 kcal/mol, but the energy barrier for the addition reaction of OPAH radical with C_2H_2 is around 20 kcal/mol. On the other hand, the O atom is likely to deactivate the reactivity if the surface sites besides the O atom are zig-zag type [48]. Therefore, the process from sub-4 nm soot to larger soot can be significantly suppressed by DME addition, resulting in the relatively higher production of sub-4 nm soot, and this influence becomes more obvious when DME mixing ratio increases.

Although soot nucleation decreases with DME addition, the strong inhibition impact of DME on the growth of soot particles may reduce the consumption of incipient soot, which results in the increased composition of sub-4 nm soot. This is one of the possible explanations of the effect of DME addition on the formation of sub-4 nm soot, and experimental validation and other reasons may need further exploration.

4. Conclusion

In this study, experimental measurements coupled with numerical simulations in premixed ethylene flame were conducted to investigate the role of dimethyl ether (DME) on soot behavior, especially the formation of incipient soot, via evaluating the particle size distributions (PSDs) and the chemical features of soot particles. DME was mixed in premixed ethylene/oxygen/argon flames at the equivalence ratio of 2.0, with the mixing ratios ranged from 0 to 30% of the total carbon fed. Two series of atmospheric pressure flames at different cold gas velocities were tested. Soot samples from the experimental flames were collected to explore the oxidation reactivity and elemental composition. Meanwhile, numerical results provided information about flame temperatures and concentration distributions of important species. Based on the experimental observations and simulation data, we draw the following conclusions:

(1) Thermal effect of DME addition is minor. The temperatures measured by thermocouples are consistent with the numerical results, and the maximum flame temperatures increase as DME mixing ratio increases with the variation within 40 K.
(2) There is a notable delay in soot evolution process ascribed to DME addition, and no indication of the synergistic effect as was detected in counterflow diffusion flames. DME addition slows down soot evolution because of the facts that soot nucleation reduced with less propargyl and acetylene, and soot oxidation enhanced with more hydroxyl and higher oxidizability. Hence, the overall production of soot particles is reduced due to DME addition.
(3) It is observed that there is a slight increase in the nascent soot with size below 4 nm in DME added flames. One possible explanation is that the existence of oxygenated-PAH (OPAH) on soot surface inhibits soot surface growth due to its relatively high reaction energy barrier. Although soot nucleation decreases because of the low production of soot precursors in the presence of DME, the strong inhibition impact by DME on the growth of soot particles reduces the consumption of incipient soot. The result of the competition between these two processes can be attributed to the increased composition of sub-4 nm soot.

Declaration of Competing Interest

The authors declare no competing financial interest.

Acknowledgments

The research was supported by the Clean Combustion Research Center (CCRC) at the King Abdullah University of Science and Technology (KAUST) (Grant No. BAS/1/1370-01-01). Yu Wang was supported by National Natural Science of Foundation of China (Grant No. 51976142) and the National Engineering Laboratory for Mobile Source Emission Control Technology (Grant No. NELM2018A11).

References

[1] E. Christensen, J. Yanowitz, M. Ratcliff, R.L. McCormick, Renewable oxygenate blending effects on gasoline properties, Energy Fuel 25 (2011) 4723–4733.
[2] O.I. Awad, R. Mamat, T.K. Ibrahim, A.T. Hammid, I.M. Yusri, M.A. Hamidi, A.M. Humada, A.F. Yusop, Overview of the oxygenated fuels in spark ignition engine: environmental and performance, Renew. Sust. Energ. Rev. 91 (2018) 394–408.
[3] S.M. Sarathy, P. Oßwald, N. Hansen, K. Kohse-Höinghaus, Alcohol combustion chemistry, Prog. Energy Combust. Sci. 44 (2014) 40–102.
[4] Y. Zhang, Y. Li, P. Liu, R. Zhan, Z. Huang, H. Lin, Invesitgation on the chemical effects of dimethyl ether and ethanol additions on PAH formation in laminar premixed ethylene flames, Fuel 256 (2019) 115809.
[5] J. Haywood, O. Boucher, Estimates of the direct and indirect radiative forcing due to tropospheric aerosols: a review, Rev. Geophys. 38 (2000) 513–543.
[6] U. Lohmann, J. Feichter, Global indirect aerosol effects a review, Atmos. Chem. Phys. 5 (2005) 715–737.
[7] C.S. McEnally, L.D. Pfefferle, Sooting tendencies of oxygenated hydrocarbons in laboratory-scale flames, Environ. Sci. Technol. 45 (2011) 2498–2503.

[8] S.S. Yoon, D.H. Anh, S.H. Chung, Synergistic effect of mixing dimethyl ether with methane, ethane, propane, and ethylene fuels on polycyclic aromatic hydrocarbon and soot formation, Combust. Flame 154 (2008) 368–377.
[9] Z. Li, H.M.F. Amin, P. Liu, Y. Wang, S.H. Chung, W.L. Roberts, Effect of dimethyl ether (DME) addition on sooting limits in counterflow diffusion flames of ethylene at elevated pressures, Combust. Flame 197 (2018) 463–470.
[10] C.S. McEnally, L.D. Pfefferle, The effects of dimethyl ether and ethanol on benzene and soot formation in ethylene nonpremixed flames, Proc. Combust. Inst. 31 (2007) 603–610.
[11] A. Serov, C. Kwak, Progress in development of direct dimethyl ether fuel cells, Appl. Catal. B: Environ. 91 (2009) 1–10.
[12] A.M. Namasivayam, T. Korakianitis, R.J. Crookes, K.D.H. Bob-Manuel, J. Olsen, Biodiesel, emulsified biodiesel and dimethyl ether as pilot fuels for natural gas fuelled engines, Appl. Energy 87 (2010) 769–778.
[13] Z. Azizi, M. Rezaeimanesh, T. Tohidian, M.R. Rahimpour, Dimethyl ether: a review of technologies and production challenges, Chem. Eng. Process. 82 (2014) 150–172.
[14] S.H. Park, C.S. Lee, Applicability of dimethyl ether (DME) in a compression ignition engine as an alternative fuel, Energy Convers. Manage. 86 (2014) 848–863.
[15] T.A. Semelsberger, R.L. Borup, H.L. Greene, Dimethyl ether (DME) as an alternative fuel, J. Power Sources 156 (2006) 497–511.
[16] J. Wu, K.H. Song, T. Litzinger, S.-Y. Lee, R. Santoro, M. Linevsky, Reduction of pah and soot in premixed ethylene-air flames by addition of dimethyl ether, Combust. Sci. Technol. 178 (2006) 837–863.
[17] M. Sirignano, M. Salamanca, A. D'Anna, The role of dimethyl ether as substituent to ethylene on particulate formation in premixed and counter-flow diffusion flames, Fuel 126 (2014) 256–262.
[18] Y. Kang, Y. Sun, X. Lu, X. Gou, S. Sun, J. Yan, Y. Song, P. Zhang, Q. Wang, X. Ji, Soot formation characteristics of ethylene premixed burner-stabilized stagnation flame with dimethyl ether addition, Energy 150 (2018) 709–721.
[19] F. Liu, S.B. Dworkin, M.J. Thomson, G.J. Smallwood, Modeling DME addition effects to fuel on PAH and soot in laminar coflow ethylene/air diffusion flames using two PAH mechanisms, Combust. Sci. Tech. 184 (2012) 966–979.
[20] F. Liu, X. He, X. Ma, Q. Zhang, M.J. Thomson, H. Guo, J. Wang, An experimental and numerical study of the effects of dimethyl ether addition to fuel on polycyclic aromatic hydrocarbon and soot formaiton in laminar coflow ethylene/air diffusion flames, Combust. Flame 158 (2011) 547–563.
[21] B.A.V. Bennett, C.S. McEnally, L.D. Pfefferle, M.D. Smooke, M.B. Colket, Computationaly and experimental study of the effects of adding dimethyl ether and ethanol to nonpremixed ethylene/air flames, Combust. Flame (2009) 1289–1302.
[22] P.H.M Hoet, I.B. Hohlfeld, O.V. Salata, Nanoparticles–known and unknown health risks, J. Nanobiotechnol. 2 (2004) 12.
[23] J.J Helble, Devito M.S, C.Y. Wu, F.L Smith, D. Marrack, Combustion aerosols: factors governing their size and composition and implications to human health, J. Air Waste Manage. Assoc. 50 (2000) 1565–1618.
[24] M. Salamanca, M. Sirignano, M. Commodo, P. Minutolo, A. D'Anna, The effect of ethanol on the particle size distributions in ethylene premixed flames, Exp. Therm. Fluid Sci. 43 (2012) 71–75.
[25] M. Sirignano, A. Ciajolo, A. D'Anna, C. Russo, Chemical features of particles generated in an ethylene/ethanol premixed flame, Energy Fuel 31 (2017) 2370–2377.
[26] C.C. Barrios, C. Martin, A. Domínguez-Sáez, P. Álvarez, M. Pujadas, J. Casanova, Effects of the addition of oxygenated fuels as additives on combustion characteristics and particle number and size distribution emissions of a TDI diesel engine, Fuel 132 (2014) 93–100.
[27] M. Sirignano, A. Ciajolo, A. D'Anna, C. Russo, Particle formation in premixed ethylene-benzene flames: An experimental and modeling study, Combust. Flame 200 (2019) 23–31.
[28] C.S. McEnally, Ü.Ö. Köylü, L.D. Pfefferle, D.E. Rosner, Soot volume fraction and temperature measurements in laminar nonpremixed flames using thermocouples, Combust. Flame 109 (1997) 701–720.
[29] C.R. Shaddix, Correcting thermocouple measurements for radiation loss: a critical review, 3rd National Heat Transfer Conference NHTC'99, Albuquerque, NM (1999).
[30] M.V. Heitor, A.L.N. Moreira, Thermocouples and sample probes for combustion studies, Prog. Energy Combust. Sci. 19 (1993) 259–278.
[31] D. Bradley, K.J. Mattews, Measurement of high gas temperatures with fine wire thermocouples, J. Mech. Eng. Sci. 10 (1968) 299–305.
[32] D. Bradley, A.G. Entwistle, Determination of the emissivity, for total radiation, of small diameter platinum-10% rhodium wires in the temperature range 600-1450 C, Br. J. Appl. Phys. 12 (1961) 708.
[33] G.E. Andrews, D. Bradley, G.F. Hundy, Hot wire anemometer calibration for measurements of small gas velocities, Int. J. Heat Mass Transfer 15 (1972) 1765–1786.
[34] Robert J. Kee, Gixon-Lewis, J. Warnatz, M.E. Coltrin, J.A. Miller, A Fortran computer code package for the evaluation of gas-phase multicomponent transport properties, Sandia Natl. Labs. 13 (1986) 80401–81887 Report SAND86-8246.
[35] A.D. Abid, J. Camacho, D.A. Sheen, H. Wang, Quantitative measurement of soot particle size distribution in premixed flames – the burner-stabilized stagnation flame approach, Combust. Flame 156 (2009) 1862–1870.
[36] J. Camacho, C. Liu, C. Gu, H. Lin, Z. Huang, Q. Tang, X. You, C. Saggese, Y. Li, H. Jung, L. Deng, I. Wlokas, H. Wang, Mobility size and mass of nascent soot particles in a benchmark premixed ethylene flame, Combust. Flame 162 (2015) 3810–3822.
[37] B. Zhao, Z. Yang, J. Wang, M.V. Johnston, H. Wang, Analysis of soot nanoparticles in a laminar premixed ethylene flame by scanning mobility particle sizer, Aerosol Sci. Tech. 37 (2003) 611–620.
[38] Z. Li, H. Wang, Drag force, diffusion coefficient, and electric mobility of small particles. I. Theory applicable to the free-molecule regime, Phys. Rev. E Stat. Nonlin. Soft. Matter Phys. 68 (2003) 061206.
[39] J. Singh, R.I.A. Patterson, M. Kraft, H. Wang, Numerical simulation and sensitivity analysis of detailed soot particle size distribution in laminar premixed ethylene flames, Combust. Flame 145 (2006) 117–127.
[40] Chemkin Pro: a chemical kinetics package for the analysis of gas-phase chemical kinetics, Reaction Desig. Release 15112 (2011) Chemkin Pro: a chemical kinetics package for the analysis of gas-phase chemical kinetics, Reaction Desig. Release 15112 (2011).
[41] S. Park, Y. Wang, S.H. Chung, S.M. Sarathy, A PAH growth mechanism and effect of alcohol addition on PAH formation in counterflow ethylene diffusion flames, Proc. Eur. Combust. Meeting (2015).
[42] W.K. Metcalfe, S.M. Burke, S.S. Ahmed, H.J. Curran, A hierarchical and comparative kinetic modeling study of C1− C2 hydrocarbon and oxygenated fuels, Int. J. Chem. Kinet. 45 (2013) 638–675.
[43] F. Yan, L. Xu, Y. Wang, S. Park, S.M. Sarathy, S.H. Chung, On the opposing effects of methanol and ethanol addition on PAH and soot formation in ethylene counterflow diffusion flames, Combust. Flame 202 (2019) 228–242.
[44] A. Raj, S.Y. Yang, D. Cha, R. Tayouo, S.H. Chung, Structural effects on the oxidation of soot particles by O2: experimental and theoretical study, Combust. Flame 160 (2013) 1812–1826.
[45] J. Song, M. Alam, A. Boehman, U. Kim, Examination of the oxidation behavior of biodiesel soot, Combust. Flame 146 (2006) 589–604.
[46] M. Alfè, B. Apicella, R. Barbella, J.N. Rouzaud, A. Tregrossi, A. Ciajolo, Structure–property relationship in nanostructures of young and mature soot in premixed flames, Proc. Combust. Inst. 32 (2009) 697–704.
[47] M. Commodo, K. Kaiser, G. De Falco, P. Minutolo, F. Schulz, A. D'Anna, L. Gross, On the early stages of soot formation: molecular structure elucidation by high-resolution atomic force microscopy, Combust. Flame 205 (2019) 154–164.
[48] P. Liu, B. Chen, Z. Li, A. Bennett, S. Sioud, S.M. Sarathy, W.L. Roberts, Evolution of oxygenated polycyclic aromatic hydrocarbon chemistry at flame temperatures, Combust. Flame 209 (2019) 441–451.